Stabilizing Solid-State Li Metal Batteries via a Poly(ethylene oxide)-LiTFSI@Boron Nitride Interfacial Layer

Songyi Han,* Hongyao Guo, Aiting Meng, Lei Zhu,* Weiping Tang, and Junchao Chen*

Na super-ionic conductor (NASICON)-structured solid electrolyte $Li_{1.3}Al_{0.3}Ti_{1.7}(PO_4)_3$ (LATP) excels in mechanical strength, ionic conductivity, and commercialization prospect, yet its incompatibility against Li metal anode typically leads to interfacial failure, significantly reducing the overall electrochemical performance of fabricated solid-state Li metal batteries (SSLMBs). Here, this issue is tackled by interposing an in situ cured poly(ethylene oxide) (PEO)-LiTFSI@BN interfacial layer between LATP and Li metal. This layer exhibits an ionic conductivity of $7.76 \times 10^{-5}\,S\,cm^{-1}$ at room temperature, robust thermostability, as well as satisfactory stability against Li metal (critical current density: $1.5\,mA\,cm^{-2}$). A Li|LATP|Li symmetric cell employing the interfacial layer demonstrates long cyclic stability over 1200 cycles with a low overpotential of $\pm 100\,mV$. Furthermore, this interfacial layer enables a $LiNi_{0.5}Co_{0.2}Mn_{0.3}O_2$ (NCM523)|LATP|Li metal SSLMB to sustain 120 cycles of operation at a cutoff voltage of 4.2 V. This work provides a practical strategy for integrating the LATP solid electrolyte into SSLMBs.

1. Introduction

Solid-state Li metal batteries (SSLMBs) are recognized as the next-generation energy storage devices as they exhibit enhanced safety, higher energy density, and extended lifespan over conventional lithium-ion batteries that rely on flammable and leakage liquid electrolytes.[1,2] This is mainly attributed to the usage of stable solid electrolytes and high-specific-energy Li metal anode.[3] Among various solid electrolytes developed, the Na super-ionic conductor (NASICON)-type solid electrolyte $Li_{1.3}Al_{0.3}Ti_{1.7}(PO_4)_3$ (LATP) presents significant advantages with regard to air stability, ionic conductivity, and cost.[4–7] However, when directly paired with Li metal anodes, the tetravalent titanium ions in LATP are easily reduced into trivalent states at

battery discharging, leading to interfacial degradation and further causing overall battery failure.[8–10] Incorporating an interfacial layer between LATP and Li metal is an effective strategy to address this issue.[11,12] Among the available material options, boron nitride (BN) thin films are promising because of their high compatibility with both LATP and Li metal.[13–16] Nevertheless, depositing thin BN films onto LATP typically relies on chemical vapor deposition, a technique that poses challenges in terms of availability. In addition, BN is an ionic insulator, significantly hindering ion conduction at the LATP/Li metal interface. Therefore, further improvements are needed for using BN as the interfacial layer.

In this work, we present a facile method for fabricating an in situ cured PEO-lithium bis(trifluoromethane sulfonimide) (LiTFSI)@BN interfacial layer by adding BN into a mixture of poly(ethylene oxide) (PEO) and lithium bis(trifluoromethane sulfonimide) (LiTFSI). By incorporating the PEO—a flexible polymer known for its high stability against Li metal[17–20]—the resulting composite film not only achieves improved physical contact between LATP and Li metal but also exhibits enhanced chemical stability at the LATP/Li metal interface. Moreover, the dissociation of LiTFSI increases the number of mobile Li^+-ions, enabling the ionic conductivity at room temperature of PEO-LiTFSI@BN film to reach $7.76 \times 10^{-5}\,S\,cm^{-1}$, and thereby reducing the interfacial resistance at the LATP/Li metal interface. With the PEO-LiTFSI@BN interfacial layer, the stabilities of LATP-based Li symmetric cell and SSLMB full cell are largely improved.

S. Han
Advanced Energy Technology and Integrated Innovation Laboratory
College of Mechanical and Electrical Engineering
Shandong Vocational College of Industry
Zibo, Shandong 256414, P. R. China
E-mail: hsyhikt@163.com

H. Guo, A. Meng, L. Zhu
Shanghai Institute of Space Power-Sources (SISP)
Shanghai Academy of Spaceflight Technology
Shanghai 200245, P. R. China
E-mail: winterzlsi@163.com

A. Meng
Hebei Key Laboratory Heavy Metal Deep Remediation in Water and Resource Reuse
School of Environmental and Chemical Engineering
Yanshan University
Qinhuangdao, Hebei 066004, P. R. China

W. Tang, J. Chen
School of Chemistry and Chemical Engineering
Shanghai Jiao Tong University
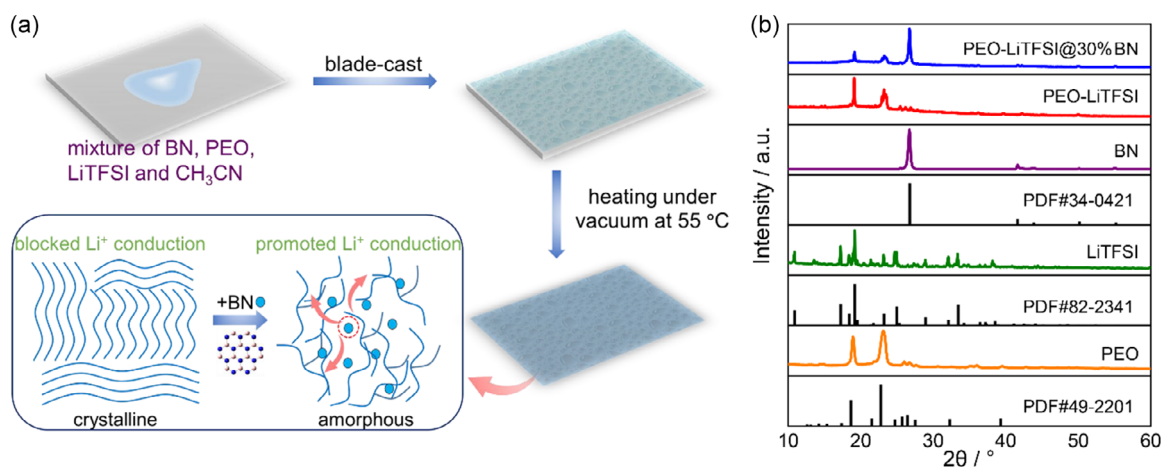Shanghai 200240, P. R. China
E-mail: junchaochen@sjtu.edu.cn

Supporting information for this article is available on the WWW under https://doi.org/10.1002/batt.202500386

2. Results and Discussion

Two PEOs with different molecular weights were compared based on their impact on the ionic conductivity of the PEO-LiTFSI@BN composite. The ionic conductivities of PEO-LiTFSI were measured using electrochemical impedance spectroscopy (EIS) for PEO with molecular weights of 0.6×10^6 and $1.0 \times 10^6\,g\,mol^{-1}$,

Batteries & Supercaps

Research Article
doi.org/10.1002/batt.202500386

Chemistry Europe
European Chemical
Societies Publishing

maintaining a PEO to LiTFSI mass ratio of 3:1. At room temperature, the ionic conductivity of the composite with $1 \times 10^6 \, g \, mol^{-1}$ PEO was $5.95 \times 10^{-6} \, S \, cm^{-1}$, compared to only $1.79 \times 10^{-6} \, S \, cm^{-1}$ for the composite with $0.6 \times 10^6 \, g \, mol^{-1}$ PEO (Figure S1, Supporting Information). Therefore, we selected PEO with a molecular weight of $1.0 \times 10^6 \, g \, mol^{-1}$ to enhance ion conduction in the PEO-based interfacial layers.
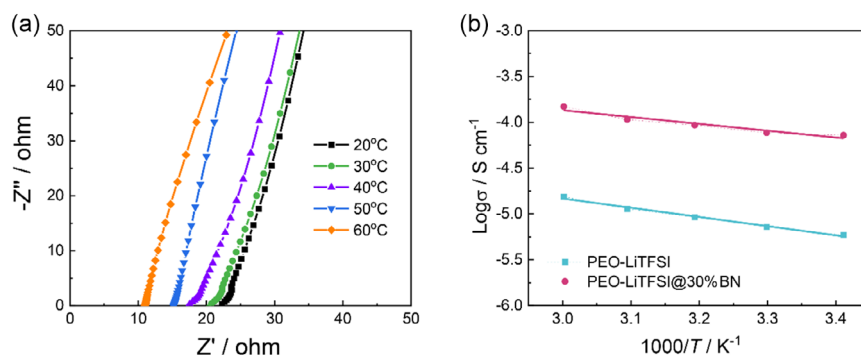
A series of PEO-LiTFSI@BN films were then prepared by the blade-cast method as shown in **Figure 1**a. The X-ray diffraction (XRD) patterns for BN, PEO, LiTFSI, PEO-LiTFSI, and the PEO-LiTFSI@BN film are presented in Figure 1b. The peaks at 18.6° and 22.8° are characteristic of pure PEO, while the peak at 26.8° corresponds to BN.[21–23] The absence of LiTFSI peaks of the PEO-LiTFSI film indicates that the LiTFSI was dissolved in the PEO matrix. In the pattern of the PEO-LiTFSI@BN film, the significant peak at 27° is attributed to BN, indicating the successful preparation of the PEO-LiTFSI@BN composite film.

The ionic conductivities of PEO-LiTFSI@BN with varying BN contents were measured by EIS (Figure S2, Supporting Information). The results show that the ionic conductivity initially increases with BN content, reaches a maximum at 30 wt%, and then decreases. At 30 wt% BN, the composite exhibits an ionic conductivity of $7.76 \times 10^{-5} \, S \, cm^{-1}$, which is nearly one order of magnitude

higher than that of PEO-LiTFSI ($5.95 \times 10^{-6} \, S \, cm^{-1}$). This enhancement may be attributed to the inorganic BN fillers, which effectively reduce the crystallinity of PEO and facilitate the movement of its chains (Figure 1a). However, further increasing the BN content adversely affects the motion of PEO chains, hindering Li+-ion transport and lowering the ionic conductivity. Additionally, as shown in **Figure 2**a, the ionic conductivity of PEO-LiTFSI@BN increases with temperature. When the temperature exceeds 60 °C, the semicircular feature in the EIS spectra disappears due to the melting of PEO,[24–26] resulting in a high conductivity of $1.38 \times 10^{-4} \, S \, cm^{-1}$. Figure S3, Supporting Information, presents the EIS spectra of the PEO-LiTFSI membrane at various temperatures. As shown in Figure 2b, the logarithmic temperature dependence of the ionic conductivity follows Arrhenius behavior. The activation energy (*Ea*) for PEO-LiTFSI@BN is determined to be 0.18 eV, lower than that of PEO-LiTFSI (0.24 eV). Notably, the reduction in activation energy for PEO-LiTFSI@BN is more pronounced across the temperature range. The observed increase in ionic conductivity and decrease in activation energy (from 0.24 to 0.18 eV) in the PEO-LiTFSI@BN composite electrolyte can be ascribed to two synergistic effects. First, adding BN nanosheets to the PEO matrix disrupts its crystallinity and generates more amorphous regions, which enhances the segmental mobility of PEO chains, and thus, promotes more

Figure 1. Preparation procedure and the texture of the PEO-LiTFSI@BN composite film. a) Schematic diagram of the preparation procedure and b) the XRD patterns of PEO, LiTFSI, BN, PEO-LiTFSI, and PEO-LiTFSI@BN.

Figure 2. Ionic conductivity measurements. a) EIS spectra of the PEO-LiTFSI@BN films recorded at temperatures ranging from 20 to 60 °C. b) Arrhenius plots comparing the ionic conductivity of PEO-LiTFSI and PEO-LiTFSI@BN.

Batteries & Supercaps

Research Article
doi.org/10.1002/batt.202500386

**Chemistry
Europe**

European Chemical
Societies Publishing
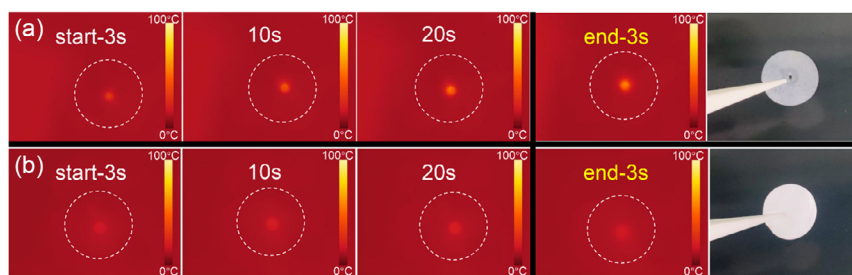
efficient Li^+ transport along the polymer backbone. Second, density functional theory calculations by Zhu et al.[15,27] show that Li^+ migration through boron vacancies in BN layers requires significantly less energy than migration via nitrogen vacancies, creating low-energy pathways for ion conduction at the interface.

The thermostability of PEO-LiTFSI and PEO-LiTFSI@BN was investigated using infrared laser irradiation, with the heat generation and conduction rates illustrated in **Figure 3**. For PEO-LiTFSI (Figure 3a), heat is rapidly absorbed and diffused throughout the film within 3 s, indicating its fast heat conduction but poor heat dissipation. After 10 s of laser irradiation, the overall temperature of PEO-LiTFSI rises to ≈50 °C, and by 20 s, the temperature at the laser center reaches the melting point of PEO, resulting in the formation of a hole. Moreover, once irradiation ceases, there is little temperature change over the subsequent 3 s, with the laser center temperature remaining at the melting point. In contrast, the temperature of PEO-LiTFSI@BN remains only slightly above room temperature after 20 s of laser irradiation (Figure 3b), and no melting is observed throughout the entire irradiation process, i.e., the film remains intact. Additionally, the surface temperature of PEO-LiTFSI@BN rapidly returns to room temperature within 3 s after the laser is turned off.
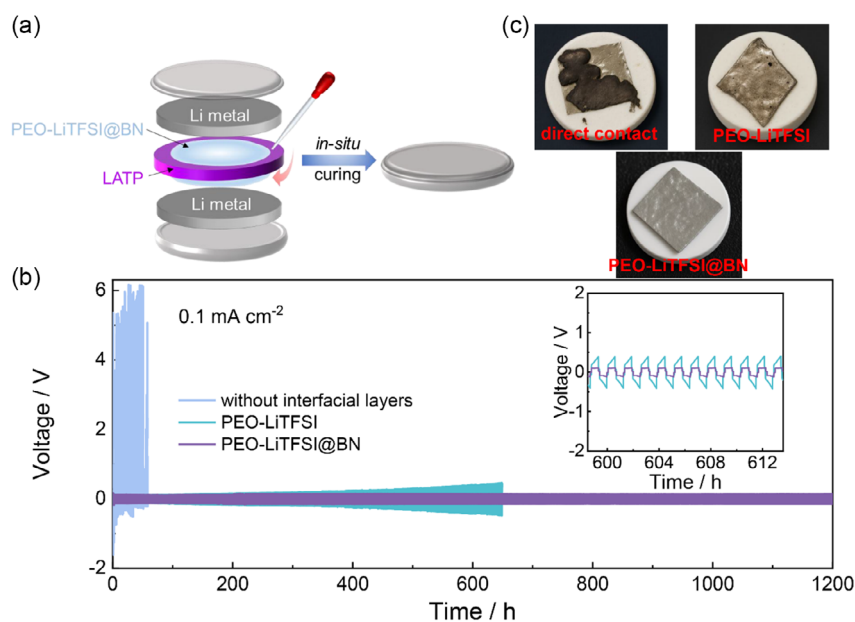
These results indicate that the addition of BN significantly enhances the heat conduction and thermostability of PEO-LiTFSI, helping to maintain its structural integrity under thermal stress.

The scanning electron microscopy (SEM) and transmission electron microscopy images of BN and LATP particles indicate that their particle sizes are ≈200 and 300 nm, respectively (Figure S4, S5, Supporting Information). The electron diffraction patterns confirm that both LATP and BN present well-defined crystal morphologies, with LATP exhibiting a rhombohedral phase (Figure S5, Supporting Information).[28] Figure S6, Supporting Information, shows the SEM images of LATP surfaces after treatment with PEO-LiTFSI and PEO-LiTFSI@BN. Compared to Figure S6a, Supporting Information, BN particles are clearly visible in Figure S6b, Supporting Information, and are uniformly dispersed within the PEO matrix. Figure S7, Supporting Information, shows that the PEO-LiTFSI@BN (C_2^+ signal) forms a uniform, continuous coating on the LATP surface, acting as an interfacial layer. Time-of-flight secondary ion mass spectrometry reveals that this layer is ≈228 nm thick.

The Li|LATP|Li symmetric cells were assembled to evaluate the stability of PEO-LiTFSI@BN interfacial layer against Li metal.

Figure 3. Thermostability measurements of a) PEO-LiTFSI and b) PEO-LiTFSI@BN films under laser irradiation.
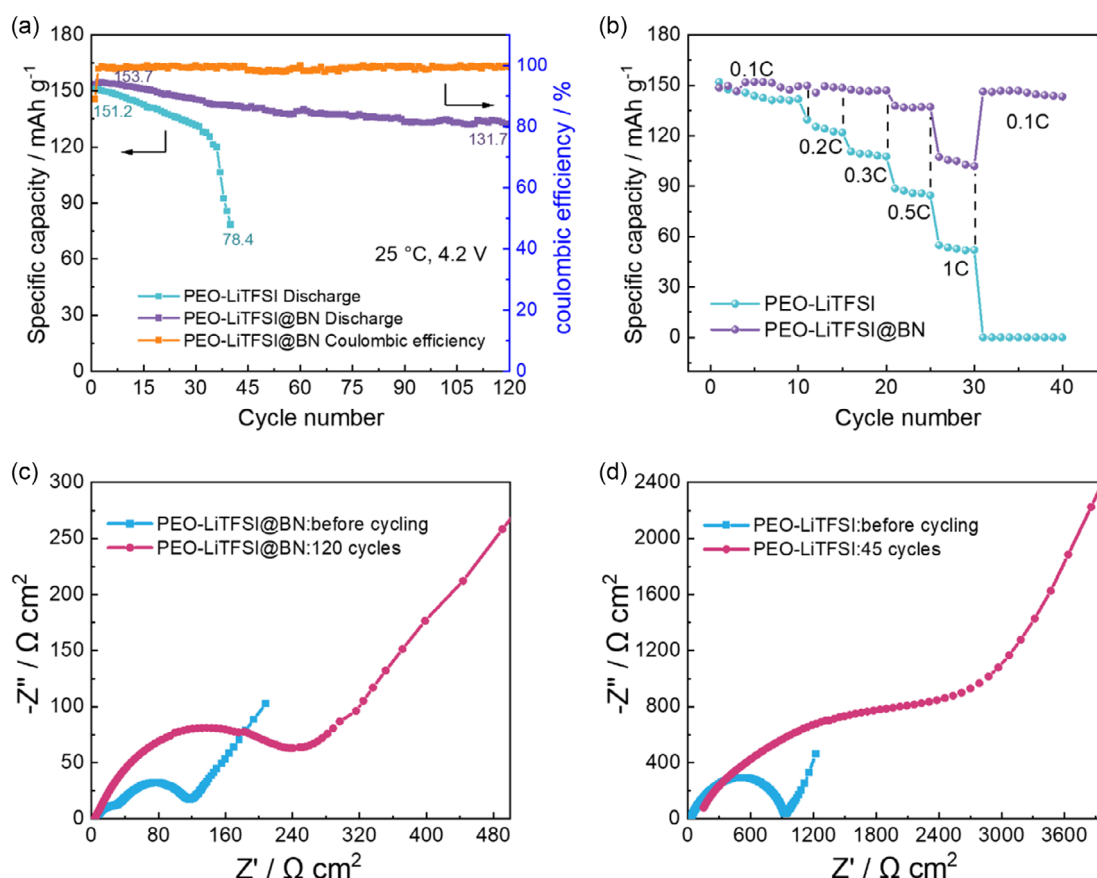

Figure 4. Stability tests of PEO-LiTFSI@BN against Li metal. a) Schematic diagram of the Li symmetric cell assembly using the PEO-LiTFSI@BN interfacial layer. b) Li stability measurements. c) Optical photograph of the Li metal stability tests.

Batteries & Supercaps

Research Article
doi.org/10.1002/batt.202500386

Chemistry Europe
European Chemical
Societies Publishing

The impedance characteristics of the Li|Li symmetric cell are shown in Figure S8, Supporting Information. As shown in **Figure 4**a, two PEO-LiTFSI@BN films were coated on both sides of the LATP to act as interfacial layers. The galvanostatic cycling curves of the symmetric cells are presented in Figure 4b. The Li|LATP|Li cell without any interfacial layer exhibits a large overpotential of 1600 mV and abnormal operation. The cell with a PEO-LiTFSI interfacial layer develops a short circuit after more than 600 h of cycling, with the overpotential increasing to 460 mV over time. In contrast, the Li|LATP|Li cell with the PEO-LiTFSI@BN interfacial layer maintains an overpotential of only 100 mV for nearly 1200 h at 0.1 mA cm^{-2}. The regular negative and positive voltage plateaus indicate uniform Li plating and stripping in the cell with the PEO-LiTFSI@BN layer. Figure S9, Supporting Information, shows that the Li|Li symmetric cell with the PEO-LiTFSI@BN layer achieves a critical current density of 1.5 mA cm^{-2}, which is sufficiently high to ensure stable lithium plating and stripping.[29,30] This result confirms that our PEO-LiTFSI@BN interlayer substantially improves interfacial stability between LATP and Li metal, making the cell suitable for practical, elevated-current operations. These results suggest that the PEO-LiTFSI@BN interfacial layer significantly improves the stability of LATP against Li metal and lowers the electrolyte/anode interface impedance.

Shown in Figure 4c, untreated LATP turns black after 30 days of contact with Li metal, indicating that side reactions occur. While LATP treated with PEO-LiTFSI shows slight discoloration, no change is observed for LATP treated with PEO-LiTFSI@BN. This further demonstrates that the PEO-LiTFSI@BN interfacial layer can effectively prevent side reactions between LATP and Li metal. The cyclic voltammetry curves (Figure S10, Supporting Information) show a pronounced current overshoot at ≈2.31 V in the Li/LATP/Au cell, which arises from the reduction of Ti^{4+} in LATP. By contrast, the Li/PEO-LiTFSI@BN-LATP/Au cell exhibits sharp, well‑defined Li stripping-plating peaks around 0 V with minimal polarization, confirming highly reversible behavior. No additional redox features appear up to 4.5 V, demonstrating that the PEO-LiTFSI@BN‑coated LATP electrolyte possesses an expanded, stable electrochemical window.

To demonstrate the practicability of the PEO-LiTFSI@BN interfacial layer in SSLMB full cells, NCM523|LATP|Li cells were assembled using the PEO-LiTFSI@BN or PEO-LiTFSI layers, and their electrochemical performance is presented in **Figure 5**. The NCM523|Li cell with the PEO-LiTFSI@BN delivers an initial capacity of 153.7 mAh g^{-1}, retains 85.7% of its capacity after 120 cycles, and maintains a coulombic efficiency above 99.5% (Figure 5a). In contrast, the capacity of the NCM523|Li cell with the

Figure 5. Electrochemical performance of NCM523|LATP|Li full cells with PEO-LiTFSI@BN and control interlayers. a) Cycling performance; b) rate performance; c) EIS curves before and after cycling with the PEO-LiTFSI@BN interfacial layer; d) EIS curves before and after cycling with the PEO-LiTFSI interfacial layer.

Batteries & Supercaps

Research Article
doi.org/10.1002/batt.202500386

Chemistry Europe
European Chemical
Societies Publishing

PEO-LiTFSI decays rapidly after ≈30 cycles, likely due to the decomposition of PEO-LiTFSI and the formation of Li dendrites.[31–33]

The cell with the PEO-LiTFSI@BN also exhibits satisfactory rate performance (Figure 5b), showing discharge capacities of 150, 146, 142, 140, and 110 mAh g^{-1} at rates of 0.1C, 0.2C, 0.3C, 0.5C, and 1C, respectively. When the current density is returned to 0.1C, the discharge capacity recovers to 150 mAh g^{-1}. In contrast, the discharge capacities of the NCM523|Li cell with the PEO-LiTFSI are significantly lower at higher rates, and its capacity decays to 0 mAh g^{-1} when the current density is reverted to 0.1C, indicating complete cell failure. This failure is attributed to irreversible interfacial degradation during high-rate cycling, where the unstable LATP/Li metal interface—lacking the mechanical and thermal reinforcement from BN—undergoes structural damage such as lithium dendrite formation and contact loss, ultimately blocking ion transport and leading to cell failure.

Figure 5c,d reveals that the resistance of the cell with the PEO-LiTFSI increases significantly from 937.3 to 2606.3 Ω cm^2, whereas the resistance of the cell with the PEO-LiTFSI@BN only changes slightly from 117.2 to 236.2 Ω cm^2. This indicates that the PEO-LiTFSI@BN interfacial layer is considerably more stable. Consequently, the satisfactory cycling and rate performance of the NCM523|Li cell with PEO-LiTFSI@BN can be primarily attributed to its high interfacial compatibility and low interfacial resistance. Overall, these results demonstrate that, compared with PEO-LiTFSI, the PEO-LiTFSI@BN interfacial layer effectively reduces interfacial resistance and prevents side reactions between LATP and Li metal.

3. Conclusion

To prevent direct contact between the Li metal anode and the LATP solid electrolyte in SSLMBs, we introduced a PEO-LiTFSI@BN interfacial layer to serve as a mediator. Compared to conventional PEO-based interface layers—comprising only PEO and Li salts—the inclusion of BN shows overall enhancements in ionic conductivity, thermostability, and stability against Li metal. A NCM523|LATP|Li SSLMB featuring the PEO-LiTFSI@BN interfacial layer delivers an initial capacity of 153.7 mAh g^{-1} and retains 85.7% of its capacity after 120 cycles. This work underscores the importance of an interfacial layer between the Li metal anode and solid electrolytes that are unstable in direct contact with it.

Acknowledgements

Conflict of Interest

The authors declare no conflict of interest.

Data Availability Statement

The data that support the findings of this study are available from the corresponding author upon reasonable request.

[1] Y. Liu, Y. Zhao, W. Lu, L. Sun, L. Lin, M. Zheng, X. Sun, H. Xie, *Nano Energy* **2021**, *88*, 106205.

[2] C. Hu, Y. Shen, L. Chen, *Curr. Opin. Electrochem.* **2020**, *22*, 51.

[3] X. Zhu, K. Wang, Y. Xu, G. Zhang, S. Li, C. Li, X. Zhang, X. Sun, X. Ge, Y. Ma, *Energy Storage Mater.* **2021**, *36*, 291.

[4] A. Mertens, S. Yu, N. Schön, H. Gunduz, H. Tempel, R. Schierholz, F. Hausen, H. Kungl, J. Granwehr, R. Eichel, *Solid State Ionics* **2017**, *309*, 180.

[5] P. Zhang, M. Matsui, Y. Takeda, O. Yamamoto, N. Imanishi, *Solid State Ionics* **2014**, *263*, 27.

[6] E. Dashjav, Q. Ma, Q. Xu, C. Tsai, M. Giarola, G. Mariotto, F. Tietz, *Solid State Ionics* **2018**, *321*, 83.

[7] W. Xiao, J. Wang, L. Fan, J. Zhang, X. Li, *Energy Storage Mater.* **2019**, *19*, 379.

[8] Y. Liu, Q. Sun, Y. Zhao, B. Wang, P. Kaghazchi, K. R. Adair, R. Li, C. Zhang, J. Liu, L. Kuo, Y. Hu, T. Sham, L. Zhang, R. Yang, S. Lu, X. Song, X. Sun, *ACS Appl. Mater. Interfaces* **2018**, *10*, 31240.

[9] P. Hartmann, T. Leichtweiss, M. R. Busche, M. Schneider, M. Reich, J. Sann, P. Adelhelm, J. Janek, *J. Phys. Chem. C* **2013**, *117*, 21064.

[10] X. Hao, Q. Zhao, S. Su, S. Zhang, J. Ma, L. Shen, Q. Yu, L. Zhao, Y. Liu, F. Kang, Y. He, *Adv. Energy Mater.* **2019**, *9*, 1901604.

[11] Y. Li, H. Wang, *Ind. Eng. Chem. Res.* **2021**, *60*, 1494.

[12] F. Ma, Y. Liu, X. Du, Q. Lu, *Solid State Ionics* **2024**, *405*, 116450.

[13] Q. Cheng, A. Li, N. Li, S. Li, A. Zangiabadi, T.-D. Li, W. Huang, A. C. Li, T. Jin, Q. Song, Xu, N. Ni, H. Zhai, M. Dontigny, K. Zaghib, X. Chuan, D. Su, K. Yan, Y. Yang, *Joule* **2019**, *3*, 1510.

[14] C. Steinborn, M. Herrmann, U. Keitel, A. Schönecker, J. Räthel, D. Rafaja, J. Eichler, *J. Eur. Ceram. Soc.* **2013**, *33*, 1225.

[15] K. Yan, H. W. Lee, T. Gao, G. Zheng, H. Yao, H. Wang, Z. Lu, Y. Zhou, Z. Liang, Z. Liu, S. Chu, Y. Cui, *Nano Lett.* **2014**, *14*, 6016.

[16] M.-T. F. Rodrigues, K. Kalaga, H. Gullapalli, G. Babu, A. L. M. Reddy, P. M. Ajayan, *Adv. Energy Mater.* **2016**, *6*, 1600218.

[17] Y. Su, F. Xu, X. Zhang, Y. Qiu, H. Wang, *Nano-Micro Lett.* **2023**, *15*, 82.

[18] Y. Li, L. Zhang, Z. Sun, G. Gao, S. Lu, M. Zhu, Y. Zhang, Z. Jia, C. Xiao, H. Bu, K. Xi, S. Ding, *J. Mater. Chem. A* **2020**, *8*, 9579-.

[19] X. Meng, D. Zhang, J. Mo, L. Liu, T. Yang, Q. Fan, Q. Zhao, R. Zhou, M. Zhang, W. Hou, W. Hu, W. Zhang, Y. Jin, B. Jiang, L. Chu, M. Li, *Appl. Surface Sci.* **2024**, *648*, 158962.

[20] D. Zhang, L. Li, X. Wu, J. Wang, Q. Li, K. Pan, J. He, *Front. Energy Res.* **2021**, *9*, 726738.

[21] L. Zhu, P. Zhu, Q. Fang, M. Jing, X. Shen, L. Yang, *Electrochim. Acta* **2018**, *292*, 718.

[22] Y. Zhu, J. Cao, H. Chen, Q. Yu, B. Li, *J. Mater. Chem. A* **2019**, *7*, 6832.

[23] M. Liu, S. Zhang, G. Li, C. Wang, B. Li, M. Li, Y. Wang, H. Ming, Y. Wen, J. Qiu, J. Chen, P. Zhao, *J. Power Sources* **2021**, *484*, 229235.

[24] Y. Li, Z. Fu, S. Lu, X. Sun, X. Zhang, L. Weng, *Chem. Eng. J.* **2022**, *440*, 135816.

[25] X. Li, X. Wang, D. Shao, L. Liu, L. Yang, *J. Appl. Polym. Sci.* **2019**, *136*, 47498.

[26] Y. Jiang, X. Yan, Z. Ma, P. Mei, W. Xiao, Q. You, Y. Zhang, *Polymers* **2018**, *10*, 1237.

[27] L. Zhu, Y. Wang, Y. Wu, W. Feng, Z. Liu, W. Tang, X. Wang, Y. Xia, *Adv. Funct. Mater.* **2022**, *32*, 2201136.

[28] Z. Cheng, T. Liu, B. Zhao, F. Shen, H. Jin, X. Han, *Energy Storage Mater.* **2021**, *34*, 388.

[29] B. Zhao, W. Ma, B. Li, X. Hu, S. Lu, X. Liu, Y. Jiang, J. Zhang, *Nano Energy* **2022**, *91*, 106643.

Batteries & Supercaps

Research Article
doi.org/10.1002/batt.202500386

Chemistry Europe
European Chemical
Societies Publishing

[30] F. Wang, M. Zhang, Z. Fang, H. Zhou, J. Wu, Z. Xu, N. Zhou, Y. Zhang, Z. Zeng, M. Wu, *Energy Storage Mater.* **2025**, *77*, 104198.

[31] Z. Zou, Y. Li, Z. Lu, D. Wang, Y. Cui, B. Guo, Y. Li, X. Liang, J. Feng, H. Li, C.-W. Nan, M. Armand, L. Chen, K. Xu, S. Shi, *Chem. Rev.* **2020**, *120*, 4169.

[32] L. Xu, J. Li, H. Shuai, Z. Luo, B. Wang, S. Fang, G. Zou, H. Hou, H. Peng, X. Ji, *J. Energy Chem.* **2022**, *67*, 524.

[33] W. Tang, S. Tang, X. Guan, X. Zhang, Q. Xiang, J. Luo, *Adv. Funct. Mater.* **2019**, *29*, 1900648.